

Active power decoupling and controlling for single-phase FACTS device

eISSN 2051-3305
Received on 29th August 2018
Accepted on 19th September 2018
E-First on 17th December 2018
doi: 10.1049/joe.2018.8823
www.ietdl.org

Junmin Zhang¹ ✉, Kaipai Liu², Yan Liu¹, Shunfan He¹, Wei Tian¹

¹Collage of Computer Science, South-Central University For Nationalities, Wuhan, People's Republic of China

²Collage of Electrical Engineering, Wuhan University, Wuhan, People's Republic of China

✉ E-mail: 173902815@qq.com

Abstract: Single-phase FACTS device has a bulky and short-life electrolytic capacitor to absorb the ripple pulsating at twice of the line frequency in DC side, resulting in lower power density. This paper introduced a structure of three-phase bridge which added an additional leg connected to an AC capacitor based on single-phase H-bridge. The 2-ripple energy of the electrolytic capacitor in single-phase H-bridge could be transformed to the film capacitor of the AC side in three-phase H bridge. The size of single-phase FACTS is reduced by ten times compared to the single-phase H-bridge. A simple control strategy had been studied, through two kinds of controllers: the digital quasi-PR controller had been used to control grid current and AC capacitor voltage and current; the two cosine controller had been used to eliminate the rest of two-ripple harmonic in the DC side, there was no controller to maintain DC voltage. The experiments verified the feasibility of the control strategy.

1 Introduction

The single-phase flexible AC transmission systems (FACTS) [1–5] have played an important role for power grids because FACTS device can improve the grid stability, controllability, and reliability, which in turn, enhance power quality and system transmission capability. As we know, all FACTS devices must set an electrolytic capacitor in DC side, resulting in short life-time, bulky volume, and low power density. The DC capacitance is given by [2]

$$C_{dc} = \frac{U_s I_s}{\omega \Delta U_{dc} U_{dc}} \quad (1)$$

where U_s is grid-rated voltage, I_s is grid-rated current, ω is grid angular frequency, U_{dc} is the average voltage in DC side, ΔU_{dc} is the allowed peak-to-peak voltage ripple.

In order to extend the FACTS's lifetime and reduce the DC capacitor bank, a great many researches have been done on topologies and control strategies [6–20]. The basic idea of topologies is adding extra-bridge arms and energy storage components such as inductor or capacitor, which permit to transform the two-ripple energy from DC electrolytic capacitor to energy storage component in AC branch. The DC capacitor is only used to filter switching ripples, thus the capacitance is been reduced. The control strategies contain three parts: DC voltage control, grid current control, and AC energy storage component voltage and current controls. The PI controller is used for DC voltage to maintain a constant. The quasi-PR controllers are used to control grid current and insure two-ripple energy transform.

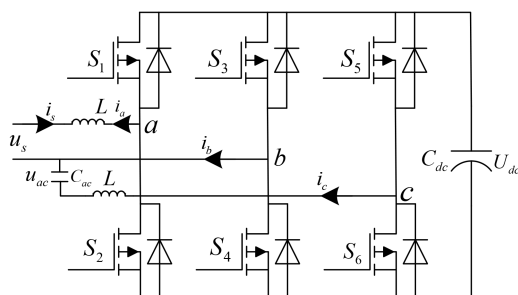


Fig. 1 Three H-bridge topology

In [13, 14], three H-bridge circuit in Fig. 1 is proposed for PWM rectifier application. By adding an auxiliary leg to single-phase H-bridge inverter, an AC film capacitor with minimal energy component is controlled to absorb two-ripple energy. The total capacitor volume is reduced by 13 times. In order to analyse remaining two-ripple in DC side and obtain the voltage and current references for AC capacitor, the control methods in [13, 14] are very complicated and time-consuming.

Here, the new topology is proposed as Fig. 1, and a novel control strategy has been studied. The DC voltage has been proved to be self-stabilised without controlling. Through a band-pass FIR filter, the remaining two-ripple energy can be analysed totally. Furthermore, the fast algorithm has been deducted. Then, the references of the AC voltage and current have been received based on total energy transform. This topology and control strategy can transfer the two-ripple energy completely, so that the electrolytic capacitor can be replaced by other kinds of ones.

2 Theoretical analysis

The novel topology is shown in Fig. 2.

Compared to Fig. 1, a filtering inductor is set in b-phase. Considering the three voltages (u_a , u_b , u_c) in Fig. 2 as controlled sources, the equivalent circuit is shown in Fig. 3.

Supposed the grid voltage and current is

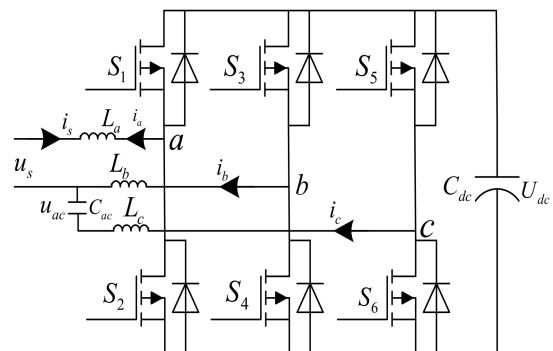


Fig. 2 Novel topology

$$\begin{cases} u_s = \sqrt{2}U_s \sin(\omega t) \\ i_s = \sqrt{2}I_s \sin(\omega t + \varphi) \end{cases} \quad (2)$$

and the voltage and current of the ac capacitor is

$$\begin{cases} u_{ac} = U_{ac} \sin(\omega t + \theta) \\ i_{ac} = I_{ac} \cos(\omega t + \theta) \\ C_{ac} = I_{ac} / \omega U_{ac} \end{cases} \quad (3)$$

The instantaneous power between *a* and *b* is

$$\begin{aligned} p_{ab} &= u_s i_s - (L_a + L_b) \frac{di_s}{dt} i_s = \frac{1}{2} U_s I_s \cos \varphi \\ &+ \frac{1}{2} U_s I_s \sin(2\omega t + \varphi - \frac{\pi}{2}) \\ &- \frac{1}{2} \omega (L_a + L_b) I_s^2 \sin(2\omega t + 2\varphi) \\ &= p_{ab_0} + \frac{1}{2} p_{ab_{2\omega}} \sin(2\omega t + \varphi_{ab}) \end{aligned} \quad (4)$$

where

$$\begin{aligned} p_{ab_0} &= \frac{1}{2} U_s I_s \cos \varphi \\ p_{ab_{2\omega}} &= \sqrt{(U_s I_s)^2 + (\omega(L_a + L_b) I_s)^2 + 2\omega(L_a + L_b) U_s I_s^2 \sin \varphi} \\ \tan \varphi_{ab} &= \frac{U_s I_s \cos \varphi - \omega(L_a + L_b) I_s^2 \sin(2\varphi)}{U_s I_s \sin \varphi - \omega(L_a + L_b) I_s^2 \cos(2\varphi)} \end{aligned}$$

In the same way, the instantaneous power between *b* and *c* is

$$\begin{aligned} p_{bc} &= u_{Cac} i_{Cac} + (L_a + L_b) \frac{di_{Cac}}{dt} i_{Cac} \\ &= \frac{1}{2} \omega C_{Cac} U_{Cac}^2 (1 - \omega^2 C_{Cac} (L_a + L_b)) \sin(2\omega t + 2\theta) \\ &= \frac{1}{2} U_{Cac}^2 \omega^2 C_{Cac}^2 \left(\frac{1}{\omega C_{Cac}} - \omega(L_a + L_b) \right) \sin(2\omega t + 2\theta) \\ &= \frac{1}{2} U_{Cac}^2 Z \sin(2\omega t + 2\theta) \end{aligned} \quad (5)$$

where

$$Z = \omega^2 C_{Cac}^2 \left(\frac{1}{\omega C_{Cac}} - \omega(L_a + L_b) \right)$$

The two-ripper energy from grid should be transformed to the C_{ac}

$$p_{ab_{2\omega}} = p_{bc} \quad (6)$$

Therefore, the magnitude and phase of AC capacitor are

$$\begin{cases} U_{ac}^* = \sqrt{\frac{p_{ab_{2\omega}}}{Z}} \\ I_{ac}^* = \frac{U_{ac}^*}{((1/\omega C_{Cac}) - \omega(L_a + L_b))} \\ \theta = \varphi_{ab}/2 \end{cases} \quad (7)$$

In primary simulink experiments, we found a few of remaining two-ripple energy in DC side. Supposed

$$u_{dc}(t) = U_{dc} + \Delta U_{\sin} \sin(2\omega t) + \Delta U_{\cos} \cos(2\omega t) \quad (8)$$

As $u_{dc}(t)$ is even function, $\Delta U_{\sin} = 0$ is Fourier decomposition. So

$$u_{dc}(t) = U_{dc} + \Delta U_{\cos} \cos(2\omega t) \quad (9)$$

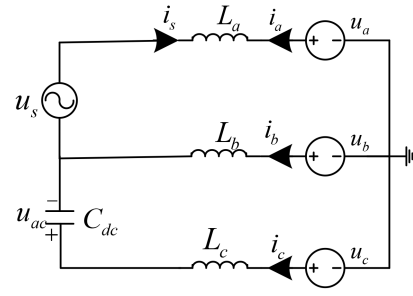


Fig. 3 Equivalent circuit of the novel topology

The instantaneous power to the DC capacitor is

$$\begin{aligned} p_{dc_r} &= C_{dc} \frac{du_{dc}}{dt} u_{dc} \\ &\approx -2\omega C_{dc} U_{dc} \Delta U_{\cos} \sin(2\omega t) \end{aligned} \quad (10)$$

the two-ripple energy should be

$$p_{ab_{2\omega}} + p_{dc_r} = p_{bc} \quad (11)$$

The voltage and current of AC capacitor are

$$\begin{cases} U_{ac}^* = \sqrt{\frac{p_{ab_{2\omega}} + p_{ab_r}}{Z}} \\ I_{ac}^* = \frac{U_{ac}^*}{((1/\omega C_{Cac}) - \omega(L_a + L_b))} \end{cases} \quad (12)$$

3 Control strategy

Fig. 4 shows the control system for single-phase FACTS device, which consists of grid current control I by controlling the magnitude of grid current and the phase angle φ , ac voltage and current control II by double close-loop, and the remaining two-ripple power analysis III. PC1 is a kind of quasi-PR controller in parts I and II, which is used to extract the two-harmonic accurately. PC2 is band-pass FIR controller, which is used to analyse the two-ripple ΔU_{\cos} .

3.1 AC capacitor control

In part II, the quasi-PR controller is used for the capacitor current in inner-loop and voltage in outer-loop. The transfer function of the controller is

$$G_{PR}(s) = K_p + \frac{2K_r \omega_c s}{s^2 + 2\omega_c s + \omega_0^2} \quad (13)$$

where ω_0 is resonance angular frequency, ω_c is cut-off angular frequency, K_p and K_r are the coefficients of the controller. The amplitude frequency characteristic diagram is in Fig. 5.

The Tusin transform is usually used to digitise the analogue quasi-PR controller. Tusin transform keeps a linear relationship in low-frequency stage from s domain to z domain. In order to guarantee the linear relationship in high-frequency, a pre-correction transform has been used

$$s = C \frac{z-1}{z+1} \quad (14)$$

where $C = \omega_0 / (\tan(\omega_0 T_s / 2))$, T_s is sample time.

Bring (14) into (13)

$$G_{PR}(z) = \frac{b_0 + b_1 z^{-1} + b_2 z^{-2}}{1 + a_1 z^{-1} + a_2 z^{-2}} \quad (15)$$

where

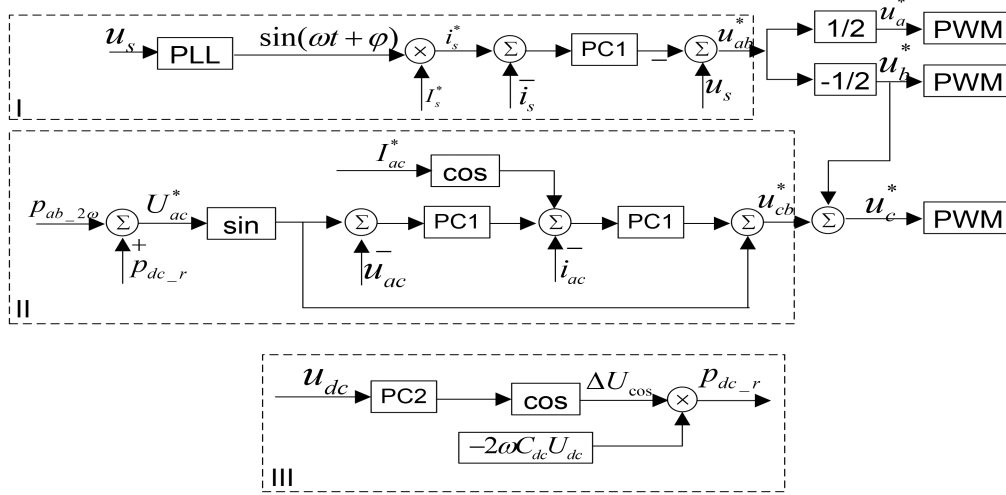


Fig. 4 Control system

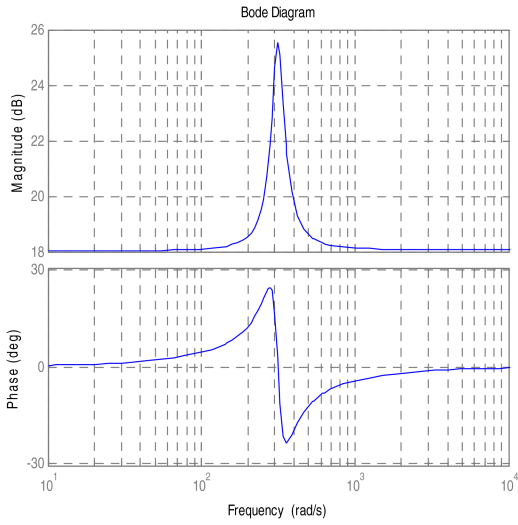


Fig. 5 The Amplitude-frequency characteristic diagram of quasi-PR

$$a_1 = \frac{2\omega_0^2 - 2C^2}{C^2 + 2\omega_c^2 C + \omega_0^2},$$

$$a_2 = \frac{C^2 - 2\omega_c^2 C + \omega_0^2}{C^2 + 2\omega_c^2 C + \omega_0^2},$$

$$b_0 = K_p + \frac{2K_r \omega_c C}{C^2 + 2\omega_c^2 C + \omega_0^2},$$

$$b_1 = \frac{K_p(2\omega_0^2 - 2C^2)}{C^2 + 2\omega_c^2 C + \omega_0^2},$$

$$b_2 = \frac{K_p(C^2 - 2\omega_c^2 C + \omega_0^2) - 2K_r \omega_c C}{C^2 + 2\omega_c^2 C + \omega_0^2}$$

The corresponding difference equation

$$y(k) = b_0 u(k) + b_1 u(k-1) + b_2 u(k-2) - a_1 y(k-1) - a_2 y(k-2) \quad (16)$$

where $u(k)$ and $y(k)$ are the input and output of the controller, respectively.

From u_{cb}^* to the AC capacitor current i_{ac} , the transfer function is

$$G_1(s) = \frac{1}{(L_b + L_c)s} \quad (17)$$

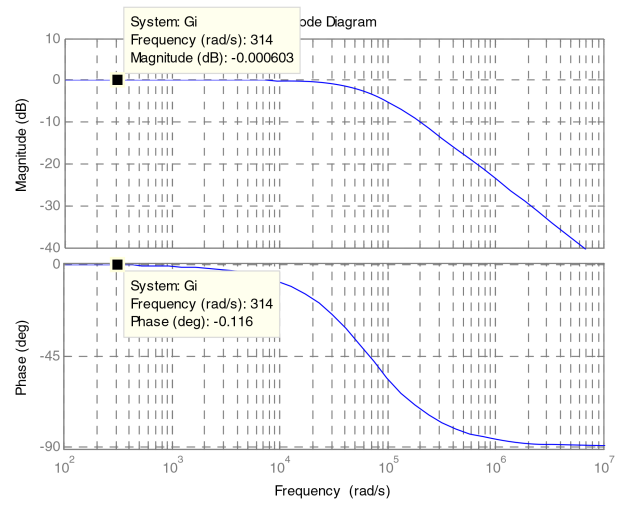


Fig. 6 Bode diagram of current close-loop

After digitising

$$G_1(z) = \frac{(1 + z^{-1})}{(L_b + L_c)(1 - z^{-1})} \quad (18)$$

The inner-loop transfer function is

$$G_{i-loop}(z) = G_{PR-i}(z)G_1(z)$$

The inner-close-loop transfer function is

$$G_i(z) = \frac{G_{i-loop}(z)}{1 + G_{i-loop}(z)} \quad (19)$$

The quasi-PR controller parameters are set: $K_p = 15$, $K_r = 22$, $\omega_c = 5$ rad/s, $\omega_0 = 314$ rad/s, and Bode plot is shown in Fig. 6.

Similarly for voltage outer-loop, from AC capacitor current to AC capacitor voltage, the digital transfer function is

$$G_2(z) = \frac{(1 + z^{-1})}{C_{ac}(1 - z^{-1})} \quad (20)$$

The inner-loop transfer function is

$$G_{v-loop}(z) = G_{PR-v}(z)G_2(z)$$

The outer-close-loop transfer function is

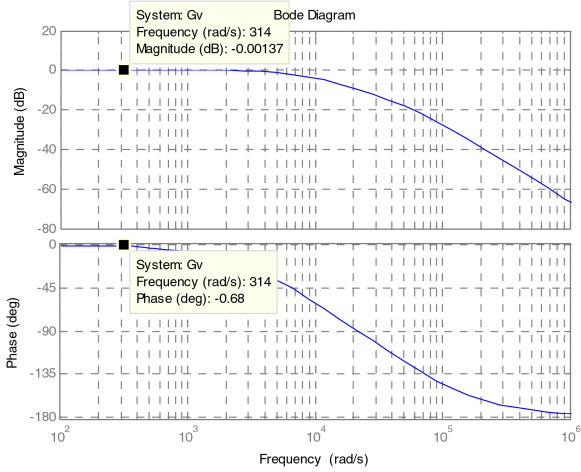


Fig. 7 Bode diagram of voltage close-loop

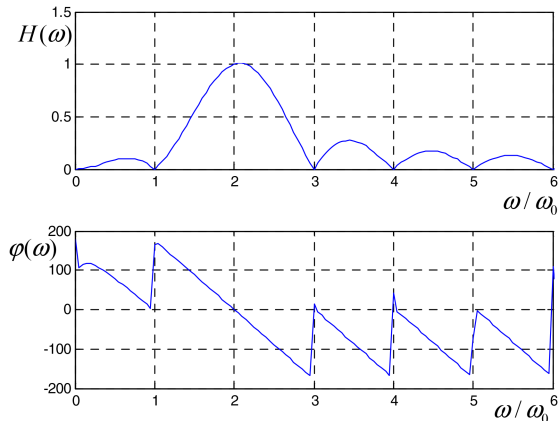


Fig. 8 The Amplitude-frequency characteristic diagram of PC2

Table 1 Key parameters

grid voltage U_s	220V(50 Hz)
grid current I_s	10 A
DC capacitance C_{dc}	50 μ F
AC capacitance C_{ac}	200 μ F
filter $L_a = L_b = L_c$	0.4 mH
switching frequency	10 kHz
φ	$\pi/2$

$$G_v(z) = \frac{G_{v_loop}(z)}{1 + G_{v_loop}(z)} \quad (21)$$

The quasi-PR controller parameters are set as $K_p = 8$, $K_r = 15$, $\omega_c = 5$ rad/s, $\omega_0 = 314$ rad/s, and Bode plot is shown in Fig. 7.

According to Figs. 6 and 7, the dual control loop obtains an acceptable bandwidth to track the reference of AC capacitor voltage and current.

3.2 DC voltage analysis

In Fig. 2, there is no load in DC side. When the device is powered on and not controlled, there is a voltage of about $\sqrt{2}U_s$ in C_{dc} . During normal operation, C_{ac} can be considered as a source, which will charge for the DC capacitor C_{dc} through the bridge arm 2, 3. At last, the voltage in C_{dc} will be maintained at $\sim\sqrt{2}(U_{ac} + U_s)$. This voltage magnitude can satisfy the work requirement. Compared to [13], there is no DC voltage control involved here.

Then in part III, the PC2 is a band-pass FIR control, the express of finite impulse response is

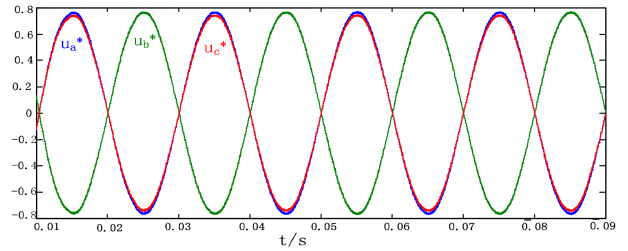


Fig. 9 The reference of control voltages

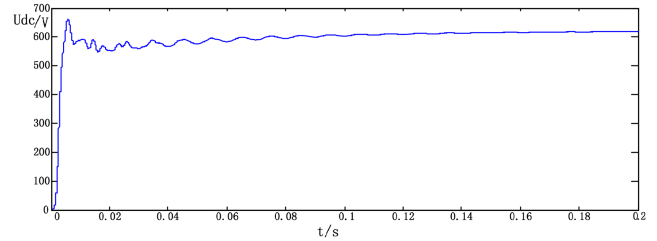


Fig. 10 The voltage in DC side

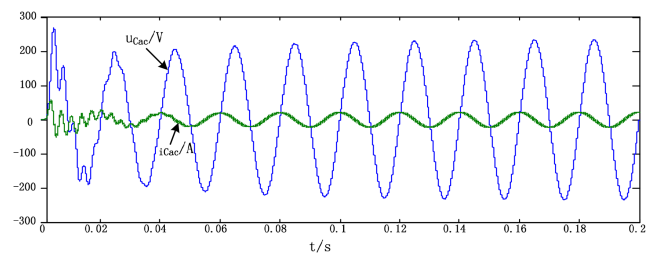


Fig. 11 The voltage and current of AC capacitor

$$h(n) = \cos\left(\frac{-4\pi(n-1)}{N}\right) \quad (22)$$

where N is sample number in a power period.

The amplitude-frequency characteristic diagram is shown in Fig. 8. The two-harmonic can be analysed without phase delay.

4 Experiment results

4.1 Simulink results

To verify the effectiveness of the proposed active power decoupling and controlling for single-phase FACTS device, we use the single-phase device which realises a variable active capacitor. A 2-kVA system is designed, the key parameters are listed in Table 1.

If the allowed DC voltage ripple is 5%, the DC capacitance is 17 mF for single-phase H-bridge system [21–23]. For the proposed three-phase H-bridge system, because two-ripple energy would be absorbed by the AC capacitor, the DC capacitor only needs to absorb switching ripple, of which the DC capacitance is 50 μ F [22]. The AC capacitance calculated based on (3) is 150 μ F. However in practice, it is designed to be 200 μ F considering a few margin. Compared to the single-phase H-bridge FACTS device, the proposed three-phase structure reduces the total size of all capacitors by ten times.

Three filter inductances L_a , L_b and L_c , if allowed the currents (including i_s and i_{Cac}) ripple is 20%, are designed to be 0.4 mH.

Figs. 9–12 show the simulation results of variable capacitor. u_a^* , u_b^* and u_c^* are the reference sine signals for controlled voltage source u_a , u_b and u_c in Fig. 9. The DC voltage eventually stabilised at about 624 V, and the remaining two-ripple has eliminated by PC2 controller. In Figs. 11 and 12, the total two-ripple energy has been transformed to the AC capacitor.

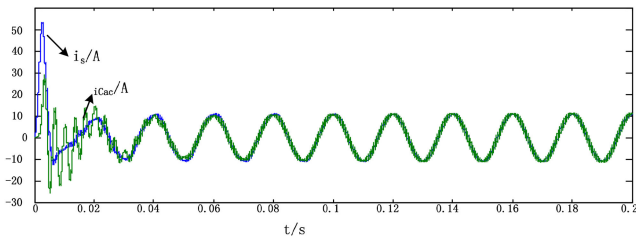


Fig. 12 The grid current and ac capacitor current

5 Conclusion

An active power decoupling and controlling for single-phase FACTS device is proposed. The two-ripple energy can be transformed from the DC capacitor in single-phase structure to the AC capacitor in three-phase structure. The bulky and short-lifetime electronic capacitor can be replaced by film capacitor. Then, FACTS device's volume can be reduced significantly and its lifetime can be extended greatly. Here, a novel strategy that include digital quasi-PR controller, band-pass FIR controller and no controller in DC voltage has proposed. The experimental results has verified the feasibility of the topology and control strategy.

6 References

- [1] Cao, D., Jiang, S., Peng, F.Z., *et al.*: 'Low cost transformer isolated boost half-bridge micro-inverter for single-phase grid-connected photovoltaic system'. Proc. IEEE 27th Annual Applied Power Electronics Conf. and Exposition, Orlando, USA, 2012, pp. 71–78
- [2] Chen, R.R., Liu, Y.T., Peng, F.Z.: 'A solid state variable capacitor with minimum capacitor', *IEEE Trans. Power Electron.*, 2017, **32**, (7), pp. 5035–5044
- [3] Liu, Y.T., Peng, F.Z.: 'Real DC capacitor-less active capacitors'. Proc. IEEE 28th Annual Applied Power Electronics Conf. and Exposition, Tampa, USA, 2017, pp. 44–51
- [4] Akagi, H., Inoue, S., Yoshii, T.: 'Control and performance of a transformerless cascade PWM STATCOM with star configuration', *IEEE Trans. Ind. Appl.*, 2007, **43**, (4), pp. 1041–1049
- [5] Yiqiao, L., Nwankpa, C.O.: 'A new type of STATCOM based on cascading voltage-source inverters with phase-shifted unipolar SPWM', *IEEE Trans. Ind. Appl.*, 1999, **35**, (5), pp. 1118–1123
- [6] Krein, P.T., Balog, R.S., Mirjafari, M.: 'Minimum energy and capacitance requirements for single-phase inverters and rectifiers using a ripple port', *IEEE Trans. Power Electron.*, 2012, **27**, (11), pp. 4690–4698
- [7] Shimizu, T., Jin, Y., Kimura, G.: 'DC ripple current reduction on a single-phase PWM voltage-source rectifier', *IEEE Trans. Ind. Appl.*, 2000, **36**, (4), pp. 1419–1429
- [8] Tsuno, K., Shimizu, T., Wada, K., *et al.*: 'Optimization of the DC ripple energy compensating circuit on a single-phase voltage source PWM rectifier'. Proc. Power Electronics Spec. Conf., Aachen, Germany, 2004, pp. 316–321
- [9] Wang, R., Wang, F., Boroyevich, D., *et al.*: 'A high power density single-phase PWM rectifier with active ripple energy storage', *IEEE Trans. Power Electron.*, 2011, **26**, (5), pp. 1430–1443
- [10] Wang, R., Wang, F., Rixin, L., *et al.*: 'Study of energy storage capacitor reduction for single phase PWM rectifier'. Proc. 24th Annu. Power Electron. Conf., Washington, DC, USA, 2009, pp. 1177–1183
- [11] Chao, K.-H., Cheng, P.-T., Shimizu, T.: 'New control methods for single phase PWM regenerative rectifier with power decoupling function'. Proc. Int. Conf. Power Electronics Drive System, Taipei, Taiwan, 2009, pp. 1091–1096
- [12] Harb, S., Balog, R.S.: 'Single-phase PWM rectifier with power decoupling ripple-port for double-line-frequency ripple cancellation'. Proc. IEEE 28th Annu. Applied Power Electronics Conf. and Exposition, Long Beach, USA, 2013, pp. 1025–1029
- [13] Li, H., Zhang, K., Zhao, H., *et al.*: 'Active power decoupling for high-power single-phase PWM rectifiers', *IEEE Trans. Power Electron.*, 2013, **28**, (3), pp. 1308–1319
- [14] Liang, S., Lu, X., Chen, R., *et al.*: 'A solid state Variable capacitor with minimum DC capacitance'. Proc. IEEE 29th Annual Applied Power Electronics Conf. and Exposition, Forth Worth, USA, 2014, pp. 3496–3501
- [15] Fan, S., Xue, Y., Zhang, K.: 'A novel active power decoupling method for single-phase photovoltaic or energy storage applications'. Proc. IEEE Energy Conversion Congress and Exposition, Raleigh, USA, 2012, pp. 2439–2446
- [16] Bush, C.R., Wang, B.: 'A single-phase current source solar inverter with reduced-size DC link'. Proc. IEEE Energy Conversion Congress and Exposition, San Jose, USA, 2009, pp. 54–59
- [17] Li, Q., Wolfs, P.: 'A review of the single phase photovoltaic module integrated converter topologies with three different DC link configurations', *IEEE Trans. Power Electron.*, 2008, **23**, (3), pp. 1320–1333
- [18] Hu, H., Harb, S., Kutkut, N., *et al.*: 'Power decoupling techniques for micro-inverters in PV systems – a review'. Proc. IEEE Energy Conversion Congress and Exposition, Atlanta, USA, 2010, pp. 3235–3240
- [19] Kyritsis, A.C., Papanikolaou, N.P., Tatakis, E.C.: 'A novel parallel active filter for current pulsation smoothing on single stage grid-connected AC-PV modules'. Proc. European Conf. on Power Electronics and Applications, Aalborg, Denmark, 2007, pp. 1–10
- [20] Liu, X., Wang, P., Loh, P. C., *et al.*: 'Six switches solution for single-phase AC/DC/AC converter with capability of second-order power mitigation in DC-link capacitor'. Proc. IEEE Energy Conversion Congress and Exposition, Phoenix, USA, 2011, pp. 1368–1375
- [21] Blaabjerg, F., Neacsu, D.O., Pedersen, J.K.: 'Adaptive SVM to compensate DC-link voltage ripple for four-switch three-phase voltage-source inverters', *IEEE Trans. Power Electron.*, 1999, **14**, (4), pp. 743–752
- [22] Kieferndorf, F.D., Forster, M., Lipo, T.A.: 'Reduction of DC-bus capacitor ripple current with PAM/PWM converter', *IEEE Trans. Ind. Appl.*, 2004, **40**, (2), pp. 607–614
- [23] Lu, X., Peng, F.Z.: 'Theoretical analysis of DC link capacitor current ripple reduction in the HEV DC-DC converter and inverter system using a carrier modulation method'. Proc. IEEE Energy Conversion Congress and Exposition, Raleigh, USA, 2012, pp. 2833–2839